Available online at www.sciencedirect.com
ScienceDirect
Trans. Nonferrous Met. Soc. China 31(2021) 2885−2898
Transactions of Nonferrous Metals Society of China
www.tnmsc.cn

Dynamic recrystallization, texture and mechanical properties of high Mg content Al−Mg alloy deformed by high strain rate rolling

Xin-yu LI[1,2], Wei-jun XIA[1,2], Ji-hua CHEN[1,2], Hong-ge YAN[1,2], Zhen-zhen LI[1,2], Bin SU[1,2], Min SONG[3]

1. College of Materials Science and Engineering, Hunan University, Changsha 410082, China;
2. Hunan Provincial Key Laboratory of Spray Deposition Technology & Application, Hunan University, Changsha 410082, China;
3. State Key Laboratory of Powder Metallurgy, Central South University, Changsha 410083, China

Received 29 November 2020; accepted 30 July 2021

Abstract: The Al−Mg alloy with high Mg addition (Al−9.2Mg−0.8Mn−0.2Zr-0.15Ti, in wt.%) was subjected to different passes (1, 2 and 4) of high strain rate rolling (HSRR), with the total thickness reduction of 72%, the rolling temperature of 400 °C and strain rate of 8.6 s^{-1}. The microstructure evolution was studied by optical microscope (OM), scanning electron microscope (SEM), electron backscattered diffraction (EBSD) and transmission electron microscope (TEM). The alloy that undergoes 2 passes of HSRR exhibits an obvious bimodal grain structure, in which the average grain sizes of the fine dynamic recrystallization (DRX) grains and the coarse non-DRX regions are 6.4 and 47.7 μm, respectively. The high strength ((507±9) MPa) and the large ductility ((24.9±1.3)%) are obtained in the alloy containing the bimodal grain distribution. The discontinuous dynamic recrystallization (DDRX) mechanism is the prominent grain refinement mechanism in the alloy subjected to 2 passes of HSRR.

Key words: Al−Mg alloy; high strain rate rolling; bimodal grain structure; dynamic recrystallization

1 Introduction

Recrystallization affected by the initial grain size, precipitation, the processing condition and stacking fault energy has mainly determined the final microstructure and mechanical properties of the alloys [1−3]. There is an increasing interest and significance in understanding the recrystallization behavior and the grain refinement mechanism of alloys [4−6].

The DRX mechanisms of the alloy during deformation contain DDRX, continuous dynamic recrystallization (CDRX) and geometric dynamic recrystallization [1,7−10]. In addition, the mechanisms are not constant and the change in the deformation condition will bring about the transformation of the mechanism of grain refinement [7,11−14]. YANUSHKEVICH et al [7] have investigated the microstructure characteristics of the austenitic stainless steel rolled at 500−1000 °C and have revealed that the new grains are generated at 800−1000 °C through the CDRX mechanism by the progressively increasing in the misorientation of the LAGBs, while the grain refinement is achieved through the CDRX mechanism by the formation of microbands at 500−700 °C. GALIYEV et al [11] have shown that the temperature range increasing from 200−250 to 300−450 °C brings about the transformation from CDRX to DDRX in the Mg−5.8Zn−0.65Zr alloy. The change of the initial grain size can also affect the DRX mechanism in the 304 austenitic stainless steel deformed by the torsion and the reduced initial

Corresponding author: Wen-jun XIA, Tel: +86-731-88823554, E-mail: xwjyxbyy@sina.com;
Ji-hua CHEN, Tel: +86-731-88823544, E-mail: jihuachen2005@163.com
DOI: 10.1016/S1003-6326(21)65726-6

grain size leads to the evolution from DDRX to CDRX [12]. DDRX and CDRX have occurred simultaneously in the high Mg alloyed Al−Mg alloy during HSRR [13], and the strain-induced deformation bands related to the high strain rate and the high Mg content play a major role. The high strain rate has similar effect as the high Mg content and the low temperature on enhancing the formation of the deformation bands. The Al−7Mg alloy subjected to the dynamic plastic deformation at low temperature experiences the CDRX process [14].

The addition of alloying element in the matrix can introduce the second phases during the casting, solution treatment and deformation processes. The reinforcement or the impediment of DRX is determined by the particle size [2,3]. NIKULIN et al [3] have revealed that Al_6Mn particles with the size of ~25 nm promote the grain refinement through CDRX, while the coarse plate-like Al_6Mn particles with the average length of ~150 nm and the width size of ~60 nm result in inhomogeneous grains due to the deficiency in the Zener drag pressure after 12 passes of equal channel angular pressing (ECAP) using route B_c. VETRANO et al [2] have shown that DRX can be enhanced by particle stimulated nucleation when the size of Al_6Mn particles is above 0.75 μm, but DRX can be effectively retarded with the introduction of the fine, coherent Al_3Sc and Al_3Zr precipitates since these precipitates can strongly inhibit the movement of dislocations and grain boundaries. Accordingly, the recrystallization temperature is noticeably increased. Therefore, the Al−Mg−X (X=Sc, Zr, Ti, Er) alloys have been widely studied to gain high strain rate superplasticity since the nano-size particles can effectively stabilize the microstructure even at high temperature [2,15,16].

The plastic anisotropy of the alloys has been basically determined by the crystallographic texture while the mechanical properties of metals and alloys have been controlled by the grain structure [17,18]. The texture evolution is closely related to the recrystallization behavior which plays the role in randomizing the texture components and weakening texture intensity [19−21]. GATTI and BHATTACHARJEE [19] have revealed that the Al−2.5Mg alloy subjected to the cold rolling shows an obvious copper texture or β-type fiber texture, while the cube texture (recrystallization texture) becomes enhanced with the higher annealing temperature and the texture intensity decreases. The recrystallization texture components are related to the recrystallization nuclei, such as grain boundaries, shear bands, and second-phase particles [20]. LIN et al [22] have shown that the microstructure refinement should be responsible for the high ductility of the alloy deformed by the cyclic extrusion compression and the texture randomization is in favor of the increasing elongation.

Many investigations have been conducted in adjusting the process condition, precipitation and stacking fault energy and so on to control the recrystallization behaviors so as to obtain the desirable grain structure and properties in the Al−Mg alloys [23−25]. SITDIKOV et al [16,23] have explored the effect of temperature on the grain refinement and mechanical behaviors of the Al−6Mg−0.4Mn−0.3Sc alloy subjected to ECAP. The alloy deformed at 450 °C exhibits a homogeneous fine-grained structure with the mean grain size of 2.8 μm, which is beneficial to achieving superior plasticity at high strain rate as the grain boundary sliding is enhanced [16], while the alloy subjected to ECAP at 300 °C shows a bimodal microstructure in which the grain sizes of the fine grains and coarse grains are 1 and 8 μm, respectively [23]. The ECAP process at room temperature for 3 passes can generate the bimodal grain distribution in the Al−7Mg alloys with the fine grains formed along the grain boundaries by the gradual evolution from LAGBs to HAGBs. The high strength and the large ductility are obtained, with the ultimate strength of ~507 MPa and the ductility of ~11% [24]. JIN and LLOYD [26] have achieved high strength and considerable elongation in the Al−3.1Mg−0.3Mn alloy with the bimodal grain distribution by asymmetric rolling and annealing, with the strength of ~250 MPa and the ductility of ~23%.

It is of great importance to understand the recrystallization behavior of the 5xxx series aluminum alloys during deformation with the increasing attention on the Al−Mg alloys due to their good weldability, high strength, low density and so on [23,24]. More attention should be focused on the Al−Mg alloy with high Mg content since the stacking fault energy is strongly decreased with the increased Mg content and the tendency to

recrystallization is increased [27−29]. The Al−Mg alloys with the fibrous structure always exhibit high strength but low ductility, while the alloys featured with the fine-grained homogenous microstructure generally show high elongations at the expense of strength [30]. Achieving a favorable balance between the strength and ductility by controlling the recrystallization behavior and the texture components attracts more and more attention [25,26]. However, most efforts are focused on the Al−Mg alloys with the Mg content lower than 5 wt.% [2,10,24]. The recrystallization mechanism and behavior of the Al−Mg alloys with higher Mg contents are rarely reported, the studies on the correlation between the microstructure characteristics and mechanical properties of the high Mg content Al−Mg alloy during HSRR are few. In the present study, the recrystallization behavior, texture evolution and mechanical properties of the Al−9.2Mg−0.8Mn−0.2Zr−0.15Ti (in wt.%) alloy deformed by different passes of HSRR were explored and the effect of the second phase particles on the recrystallization behavior was also studied.

2 Experimental

The direct-chill Al−9.2Mg−0.8Mn−0.2Zr−0.15Ti alloy castings were subjected to the homogenization treatment (400 °C, 24 h) followed by water quenching at room temperature. The homogenized alloys with sizes of 90 mm × 60 mm × 10 mm were then subjected to different passes (1, 2 and 4) of high strain rate rolling at 400 °C and the inter-pass holding time of 5 min. The data of the inter-pass rolling reduction during deformation are shown in Table 1. The strain rate $\dot{\varepsilon}$ was calculated by

$$\dot{\varepsilon}=\frac{H-h}{H}\frac{v}{\sqrt{R(H-h)}}$$

where H, h, v and R are critical thickness, final thickness, roll circumferential speed and roll radius, respectively. Thus, we can control the v to make the rolling strain rate constant, i.e. 8.6 s^{-1}. The alloys subjected to 1 pass, 2 passes, and 4 passes of HSRR were labeled as 1P, 2P and 4P samples, respectively. It should be noted that severe cracks occur in the 1P sample, which is possibly related to the Mg segregation at the grain boundaries or the stress release [31]. The alloy deformed by 4 passes of conventional rolling (CR) was selected for comparison.

Table1 Data of inter-pass thickness reduction

Sample	Thickness reduction/%	Total thickness reduction/%
1P	72	72
2P	40, 53	72
4P	20, 25, 33, 30	72

The as-rolled samples were observed by OM after etching by the Keller reagent (1 mL HF + 1.5 mL HCl + 2.5 mL HNO_3 + 95 mL H_2O). The samples for EBSD and TEM observations were subjected to the twin-jet electro-polishing, with the solution of 30vol.%HNO_3+70vol.%CH_3OH, the measured voltage of 13 V, the temperature of −30 °C and the time of 2−3 min. The TEM analysis was performed by a Titan G2 60−300 transmission electron microscope. The EBSD observation was undertaken by a ZEISS EVO MA10 scanning electron microscope (SEM) equipped with the Oxford EBSD detector, with the performed voltage of 20 kV, the tilt angle of 70° and the scanning step of 0.8 μm. It should be noted that the 4P sample was subjected to a low-temperature annealing treatment (250 °C for 30 min) before the EBSD testing since the low intensities of the Kikuchi diffraction patterns related to the high internal stress make the EBSD observation difficult. Therefore, the EBSD result is discounted to express the as-deformed microstructure of the 4P sample. The tensile samples with the gauge section of 25 mm × 6 mm × 2.8 mm were cut along the rolling direction and tested at room temperature with the tensile strain rate of 2×10^{-3} s^{-1}.

3 Results and discussion

3.1 Microstructures

The TEM, SEM images and EDS results of the second phases in the homogenized alloys are shown in Fig. 1. The homogenized alloy mostly consists of α(Al), Al_6Mn and some coarse Al_6(Fe,Mn) phases. The remnant Al_6(Fe,Mn) phase during the homogenization treatment is ascribed to its high melting point. The alloy contains rod-like Al_6Mn particles with the length of (144±30) nm and width of (74±12) nm. The orthorhombic Al_6Mn phases have been detected in the aluminum implanted with

(0−3.5) at.% Mn and followed by annealing treatment at 460 °C for 4 h [32]. The transformation among Al_6Mn, α-$Al_{12}Mn_3Si$ and quasicrystalline phases related to the impurity Si element, Mn content and annealing temperature has been observed in the Mn-bearing aluminum based alloys during the annealing treatment [33,34]. NIKULIN et al [3] have revealed that the Al−5.4Mg−0.5Mn−0.1Zr alloy homogenized at 360 °C for 6 h is featured with fine Al_6Mn particles with the size of ~25 nm, whereas the alloy homogenized at (440 °C, 12 h) + (500 °C, 12 h) contains the coarser plate-like Al_6Mn particles.

The microstructures of the alloys rolled in different states are shown in Fig. 2. No new DRX grains are detected in the CR and 4P sample and the grains are strongly elongated along the rolling direction (RD), which reveals that only recovery occurs during the rolling processes. The 2P sample contains more complicated grain structure in comparison with the 4P sample and is composed of the coarse DRX grains along the initial grain boundaries, some fine-grained bands and the non-DRX regions. The 1P sample exhibits a distinct duplex grain distribution, with the average size of the honeycomb-like DRX grains of (3.1±0.7) μm and the island-like DRX grains of (1.2±0.3) μm.

The fraction of the DRX grains increases with the decreased rolling pass during HSRR, namely, the higher rolling reduction can effectively improve the DRX. NAM et al [35] have studied the corrosion behaviors of hot-extruded Al−Mg alloys and have found that an increase in Mg content can lead to finer grains and better pitting resistance. CHOI et al [36] have revealed the behavior of β phase (Al_3Mg_2) in AA5083 during friction stir welding and have shown that the transformation of the elongated coarse grains into the fine DRX grains can effectively impede the precipitation of Al_3Mg_2 phases. The uniform, fine DRX grains in 1P sample have potential to enhance the elongation and corrosion resistance. Different DRX grain structures in the 1P and 2P samples are possibly due to different nucleation points or different grain refinement mechanisms. WU et al [37] have shown a horseshoe-like grain structure in the ZK60 alloy subjected to multiple forging. The fine DRX grains occur at the initial grain cores owing to the twin-induced DRX mechanism, while the coarse DRX grains are generated along the original grain boundaries due to the grain rotation DRX mechanism.

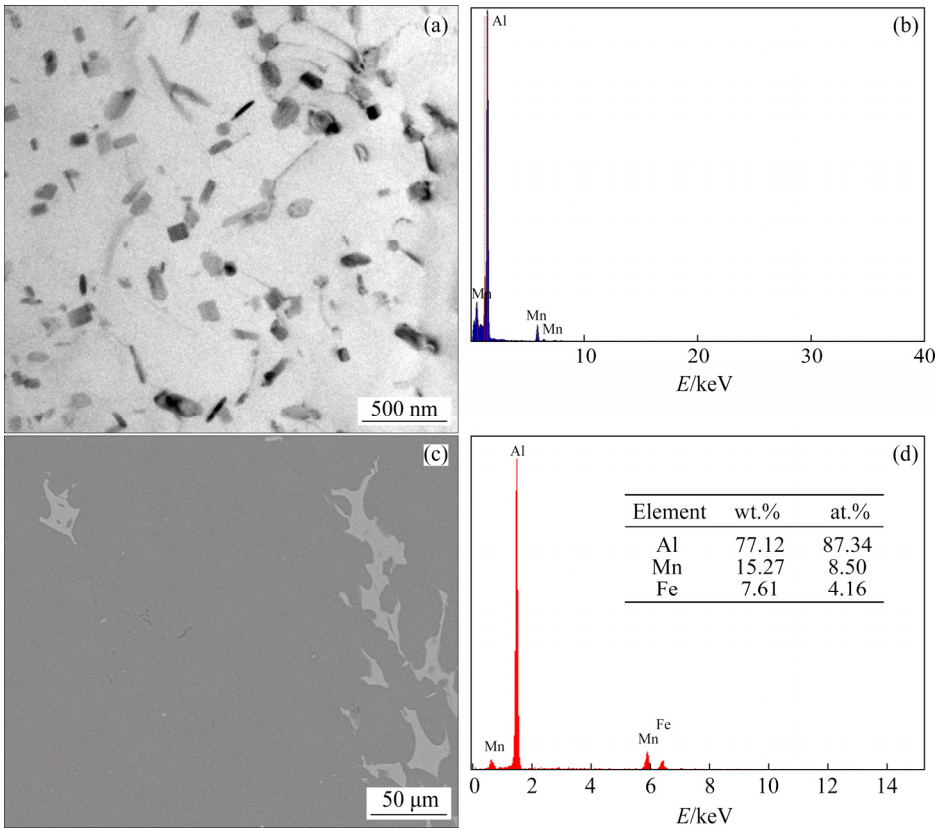

Fig. 1 TEM (a) and SEM (c) images, and EDS results (b, d) of second phases in homogenized alloys

The EBSD images and the corresponding overall boundary misorientation distributions of the alloys in different states are shown in Fig. 3. The fraction of HAGBs (F_{HAGBs}) and the average sub-boundary misorientation (θ_{AV}) increase with the decreased rolling passes. The F_{HAGBs} increases from 7.2% to 95.6% with the rolling pass decreasing from 4 to 1, while the value of θ_{AV} increases from 5.5° to 39.6°. The peaks in the misorientation angle distribution of the alloy in different states are also different and the peak of 30°−60° is detected in the 1P sample, indicating that a nearly random orientation is developed in the alloy. The 4P sample shows the elongated and flat grain structure and almost no new grains are observed.

With less rolling passes, the fraction of DRX grains increases and more homogenous grain distribution occurs. A uniform fine-grained

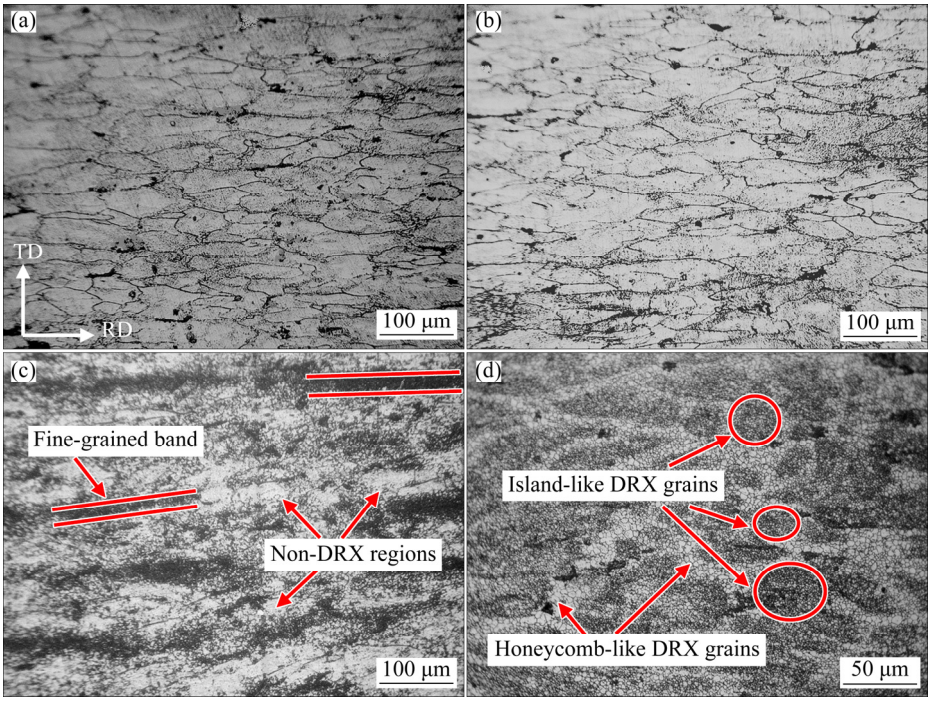

Fig. 2 Microstructures of alloys rolled in different states: (a) CR; (b) 4P; (c) 2P; (d) 1P (RD is the rolling direction; TD is the transverse direction)

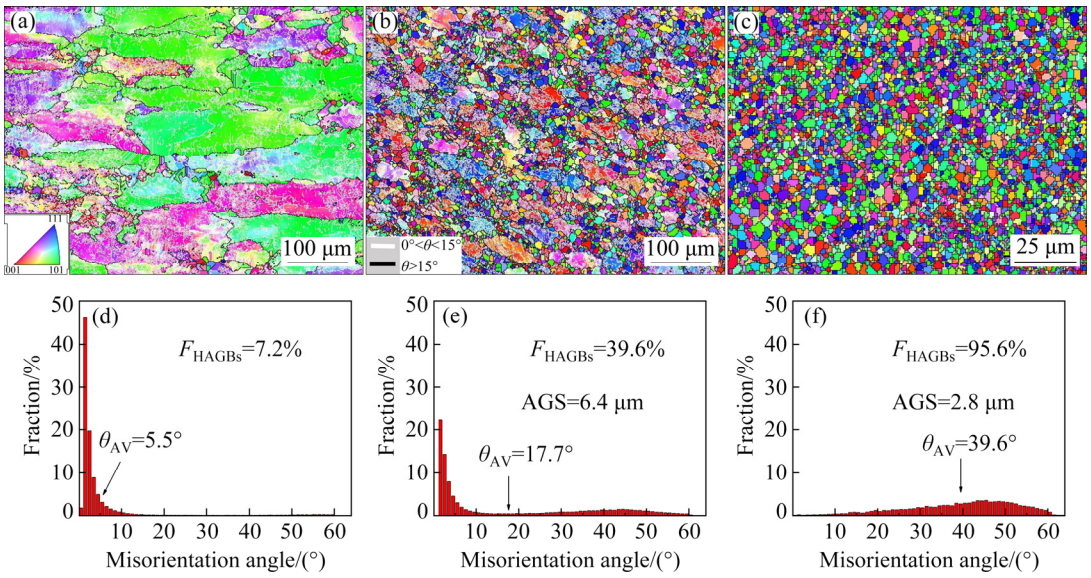

Fig. 3 EBSD images (a−c) and overall boundary misorientation distributions (d−f) of alloys rolled in different states: (a, d) 4P; (b, e) 2P; (c, f) 1P (The white and black lines depict differences between neighboring grid points $0°<\theta<15°$ and $\theta>15°$, respectively; AGS is the average size of the DRX grains)

microstructure with the average DRX grain size of 2.8 μm is detected in the 1P sample. It is worth noting that an obvious bimodal grain structure is developed in the 2P sample, in which the fine DRX grains with the average size of 6.4 μm and the coarse non-DRX regions with the average size of 47.7 μm are formed. It can be observed that the coarse non-DRX regions contain many structures with low angle grain boundaries, indicating that the high dislocation density is involved in the non-DRX regions. Some incomplete grain boundaries with HAGBs are also detected in the interior of the non-DRX regions, revealing that the high fraction DRX grains are formed as the deformation proceeds.

Generating a bimodal grain structure has been the core of the investigation to gain both high strength and large ductility since the ultrafine or nanostructure grains can provide high strength by grain boundary strengthening and the coarse grains can supply the required work hardening ability [24,38]. However, the bimodal grain structure with the fine grains in micron-scale in the Al−Mg alloy has been rarely reported since the strength is not sensitive for the alloy with the grains in the micro-scale size related to the low Hall−Petch slope [39]. KAIBYSHEV et al [40] have shown that the higher strength and the larger ductility are obtained in the Al−5Mg−0.18Mn−0.2Sc−0.08Zr alloy with the bimodal structure (with the grain size of 1.6 μm) than that with the uniform fine-gained microstructure (with the average grain size of 1.2 μm). The high strength is ascribed to the high dislocation density. The fine grains are beneficial to achieving high elongation and high strain rate super-plasticity due to the high work hardening ability and the enhanced grain boundary sliding [15,41]. The alloy contains a bimodal structure, in which the fine grains are in micron-scale size, resulting in high strength and satisfactory ductility.

3.2 Texture characteristics

To understand the texture components of the alloys deformed by different passes of HSRR, the ODFs of the alloy in different states are conducted and shown in Fig. 4. The 4P sample exhibits the distinct deformation texture components, i.e. β fiber texture which runs from the brass (B) texture $\{011\}\langle 211\rangle$ through the S texture $\{123\}\langle 634\rangle$ to the copper (C) texture $\{112\}\langle 111\rangle$. The cube texture $\{001\}\langle 100\rangle$ is the dominant texture component in the 2P sample, while the texture is close to the random state in the 1P sample. The maximum values of the texture intensity of the 4P, 2P and 1P samples are 9.55, 3.31 and 1.65, respectively. XIAO et al [42] have revealed that the alloys with fine grains in random orientation are beneficial to the uniform stress distribution when the loading is applied and the higher external loading is required to yield the fine grains and achieve the ductility improvement. A nearly random texture component has been generally reported in the annealed or homogenized states since the weak texture always indicates the low dislocation density and the weak mechanical property anisotropy in the alloy [43]. The DRX grains developed by severe plastic deformation processes are usually in a non-equilibrium state since high stored energy or high dislocation density is involved with the grains [44]. The nearly random texture component in the 1P sample should be ascribed to the enhanced DRX by HSRR with the high rolling reduction.

3.3 Dislocation structure and precipitation

The TEM images of the alloys in different states are shown in Fig. 5. The HAADF-STEM image and elemental mapping of the 2P sample are shown in Fig. 6. The dislocation tangles and the ill-defined (sub)grain boundaries containing dense dislocations are detected in 4P sample, while the well-defined sub-grains and DRX grains with lower dislocation density are obviously shown in the 2P and 1P samples. This means that the increased rolling reduction in HSRR can enhance the DRX process. The fine Al_6Mn precipitates are observed along the grain (sub-grain) boundaries or in the grain interiors, which can effectively pin the grain (sub-grain) boundaries and dislocations due to the strong Zener drag pressure. The incoherent equiaxed Al_6Mn particles with the average size of ~25 nm exert higher Zener drag pressure than the coarse plate-like Al_6Mn particles with the average sizes of ~150 nm and ~60 nm in the longitudinal and transversal directions, respectively. The grain growth occurs owing to the weak Zener drag pressure of the particles [3].

To understand the effect of the first-pass rolling deformation and inter-pass annealing on the DRX behavior in the 2P sample, the sheet subjected

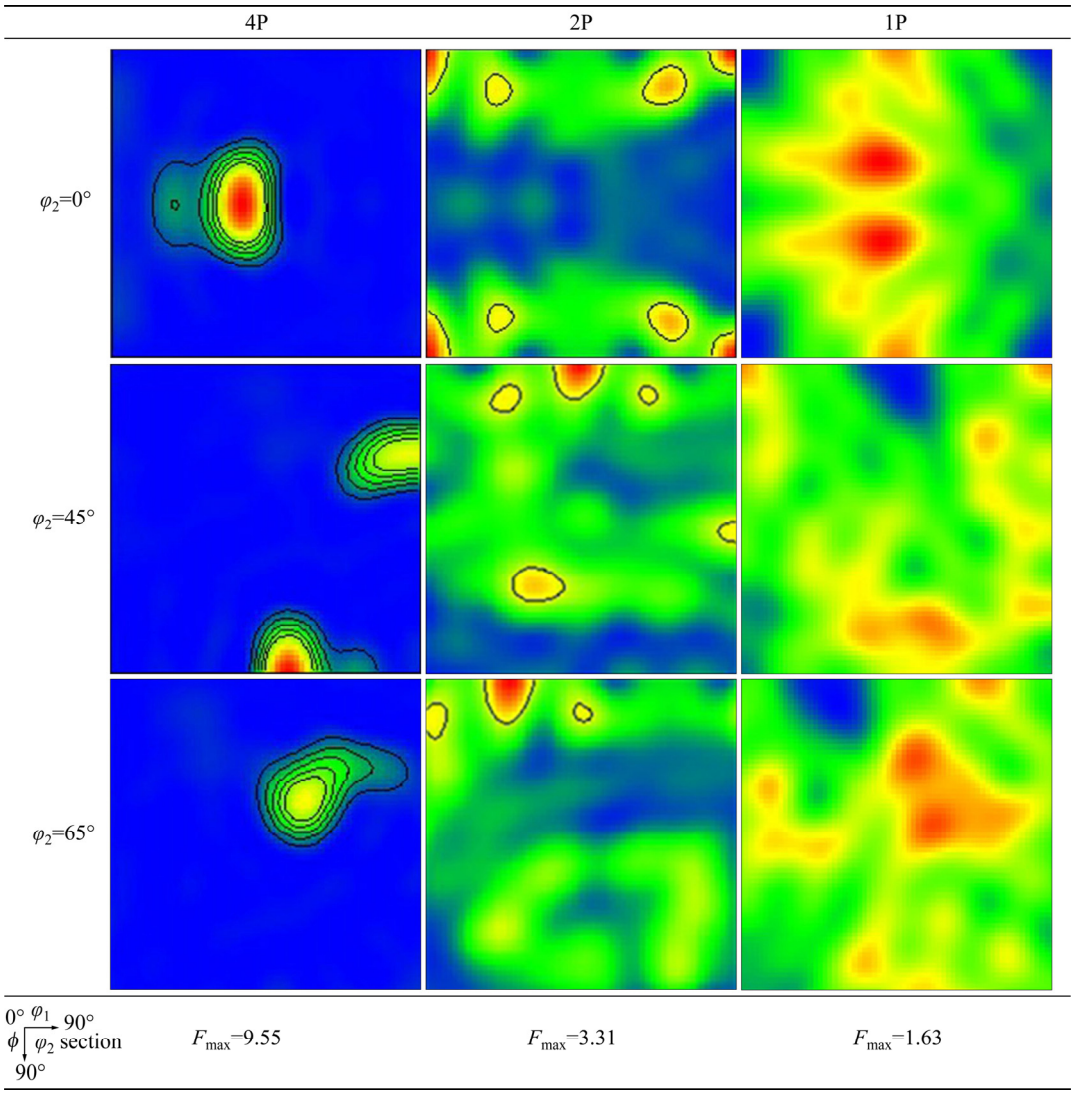

Fig. 4 ODFs of φ_2=0°, 45° and 65° sections of alloys in different states

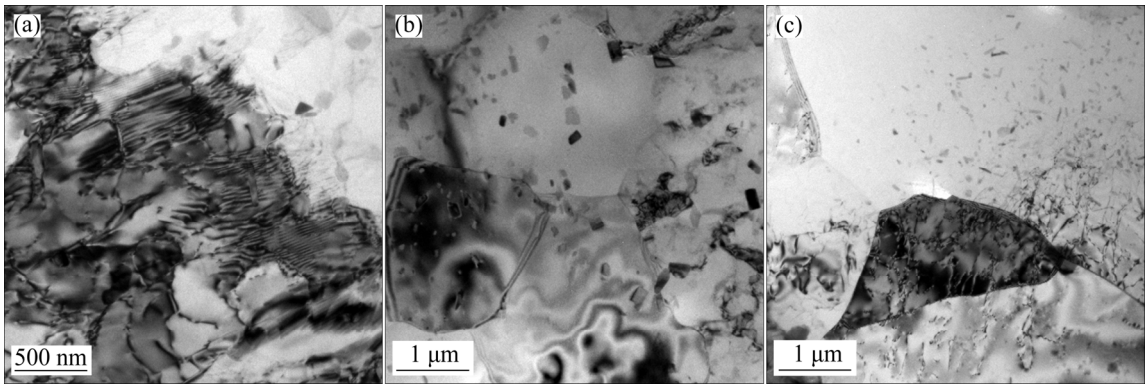

Fig. 5 TEM images of alloys rolled in different states: (a) 4P; (b) 2P; (c) 1P

to HSRR with the rolling reduction of 40% underwent an annealing treatment at 400 °C. The Vickers hardness−annealing time curve and the corresponding OM images are shown in Fig. 7.

The hardness decreases with the longer annealing time and is nearly stable when the annealing time is not less than 30 min. The new grains are not detected in the OM images of the

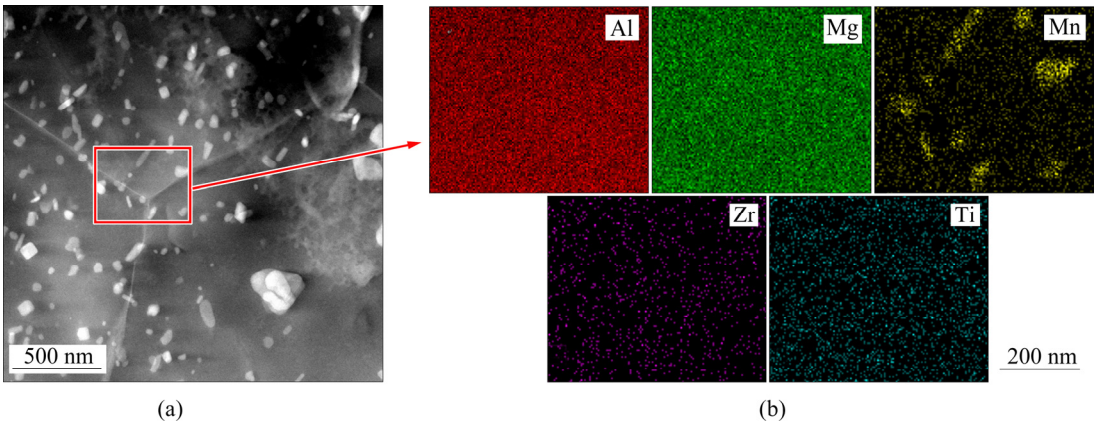

Fig. 6 HAADF-STEM image (a) and elemental mapping (b) of 2P sample

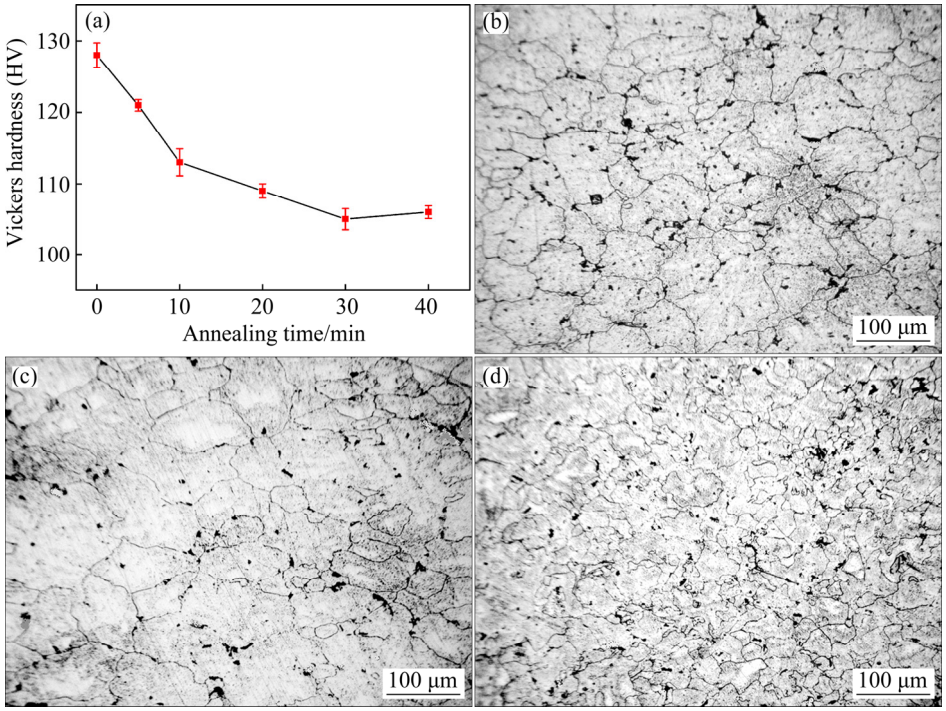

Fig. 7 Vickers microhardness−annealing time curve of alloy subjected to HSRR with rolling reduction of 40% (a), OM images of HSRRed sheet (b), sheet subjected to annealing treatment at 400 °C for 5 min (c) and 40 min (d)

HSRRed sheet and the sheet subjected to annealing treatment at 400 °C for 5 min, while finer grains are observed in the sheet subjected to annealing treatment for 40 min. The hardness decrease is closely related to the occurrence of recovery and recrystallization as the both softening processes can consume stored energy and dislocations [45]. The obvious hardness decrease in the sheet subjected to annealing treatment for 40 min is closely related to the static recrystallization process, while the slight hardness decrease in the sheet subjected to annealing treatment for 5 min is ascribed to the recovery process. The absence of the new grains during annealing treatment for 5 min is mainly attributed to the low storage energy generated during the deformation and the Zener drag pressure of the precipitation on the dislocations and grain boundaries. Thus, only recovery occurs during the reheating process and the new grains developed in the 2P sample are due to DRX instead of static recrystallization.

As shown in Fig. 2(c) and Fig. 3(b), the DRX grains are primarily formed along the initial grain boundaries and the obvious necklace-like structure is detected, indicating that the DDRX mechanism plays the significant role in the alloy subjected to 2

passes of HSRR. The TEM images showing the sub-grains, precipitates and dislocations of the 2P sample are shown in Fig. 8.

The bulging of the part of the pre-existing grain boundary and the formation of sub-grains along the grain boundary are shown in Figs. 8(a) and (b), and both of which are the distinctive features of the occurrence of DDRX [1]. The dislocations can be effectively captured by HAGBs and the accumulation of dislocation or a lot of misorientation gradients develop near the grain boundary. The formation of sub-grains and new grains occur along the original boundary due to the enough driving force [1,11]. The fine-grained bands in the 2P sample probably result from DRX by introducing the deformation bands at high strain and high strain rate. The formation of deformation bands is primarily decided by the grain orientation. The grains with the multiple slip orientation are stable against the lattice rotations and can undergo the uniform plastic deformation without subdivision, while the grain refinement or the interior deformation bands occur to accommodate the deformation strain in the grains lack of cross slip [14].

The relationship between dislocations and precipitates is shown in Figs. 8(c) and (d). The particles can impede the movement of dislocations owing to the efficient Zener drag pressure, and the dislocations can bypass or cut the particles when the loading is applied. The Al_6Mn precipitates with the size less than 200 nm do not enhance the DRX processes by particle stimulated nucleation (PSN) [46]. But they can improve the accumulation of dislocations by hindering the movement of dislocations or dynamic recovery, which can promote the development of DRX to some degree. The fine Al_6Mn precipitates can provide high strength due to precipitation strengthening [46,47]. The coarse $Al_6(Fe,Mn)$ particles with sizes above 1 μm are impurity phases and the number is small. A majority of Mn atoms exist in the Al_6Mn phase in the alloy, and the role of the $Al_6(Fe,Mn)$ particles on the DRX is limited.

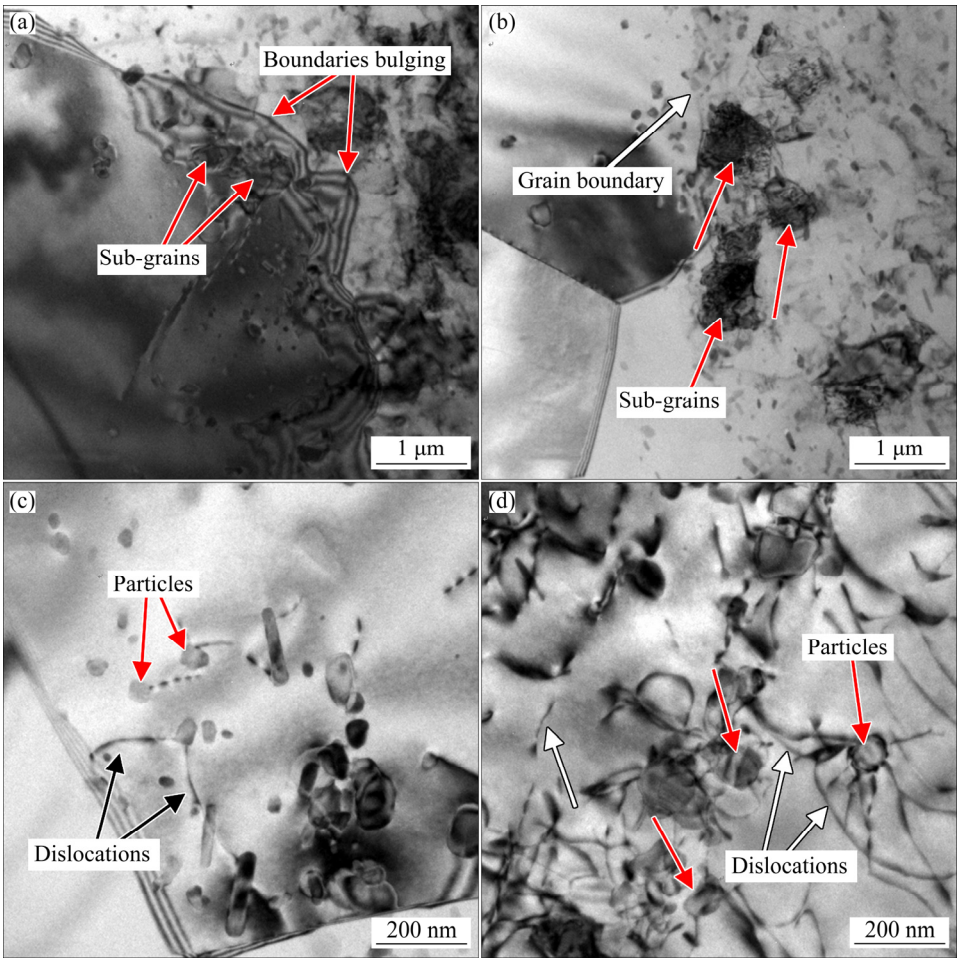

Fig. 8 TEM images showing sub-grain, precipitates and dislocations of 2P sample: (a, b) Sub-grains along initial grain boundaries; (c, d) Relationship between dislocations and precipitates

3.4 Mechanical properties

The engineering stress−engineering strain, true stress−true strain and work hardening rate−true strain curves of the alloys in different states are shown in Fig. 9. The mechanical properties of the as-studied alloys in different states and other Al−Mg alloys subjected to diverse plastic deformation are shown in Table 2 [24,39,48,49].

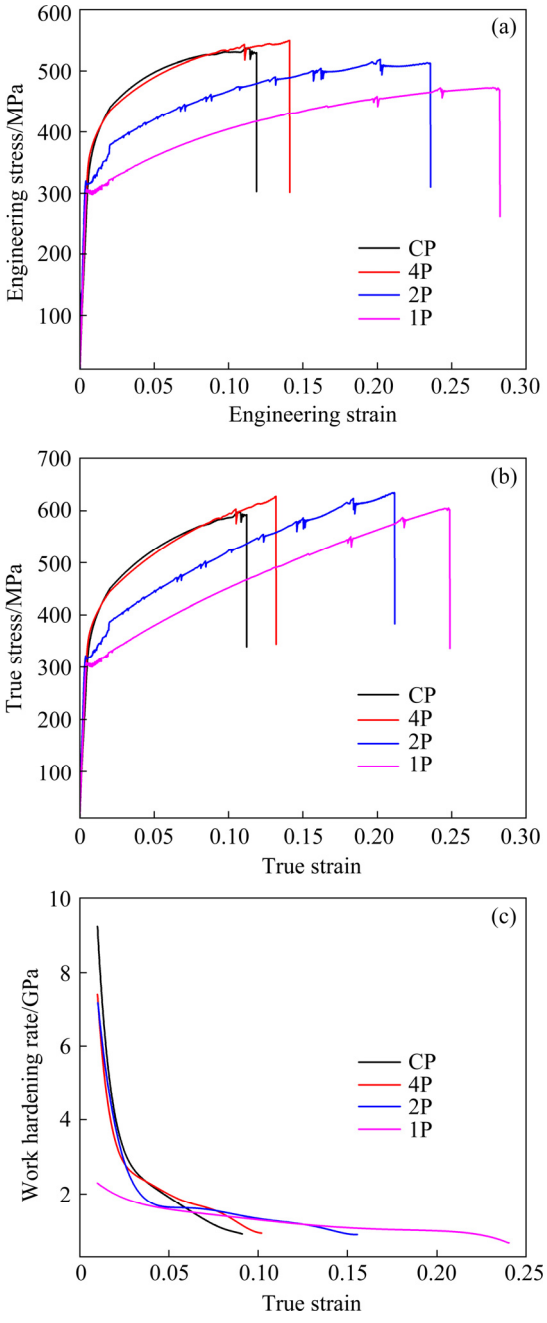

Fig. 9 Engineering stress−engineering strain (a), true stress−true strain (b), and work hardening rate−true strain (c) curves of alloys rolled in different states

The 4P sheet exhibits the highest strength but lower ductility, while the 1P alloy shows the highest elongation to failure at the expense of strength. The alloy subjected to 2 passes of HSRR exhibits good combination of mechanical properties, with ultimate tensile strength (UTS) of (507±9) MPa and the elongation to failure of (24.9±1.3)%. The 4P sample shows slightly higher strength than the CR sample since the high strain rate can enhance the generation of dislocations and thus a higher work hardening is obtained. The effects of strain and strain rate on the microstructure evolution and mechanical properties of metals and alloys are weakened with the increasing deformation temperature since the recovery process is enhanced [50].

Being a softening mechanism, DRX can immensely consume the free energy of the alloy generated during the plastic deformation, and thus the dislocation density or work hardening decreases [1,25,40]. The face-centered cubic (FCC) and body-centered cubic (BCC) metals show smaller effect of grain size on the yield strength than the hexagonal close-packed (HCP) metals due to their low Hall−Petch slopes [40,51]. Thus, the micron-sized fine grains cannot contribute enough strength in the 1P sample. But the occurrence of DRX can effectively weaken the texture and dislocation tangles, which is indicated by Fig. 4 and Fig. 5. The texture intensity decreases from 9.55 to 1.65 with the HSRR passes ranging from 4 to 1, and a nearly random orientation develops with the annihilation of the β fiber texture. The dislocation tangles disappear and are replaced by the equiaxed DRX grains with a few dislocations in the 1P alloy. The stress concentration is delayed in the alloy with the weak texture intensity since a uniform stress distribution occurs during the tensile testing [42]. A full DRX microstructure is obtained in the 1P sample, which is mainly related to the continuous dynamic recrystallization. As shown in Fig. 9(c), the fine grains can afford enough dislocation storage ability and thus the high work hardening rate is realized at the higher strain. Therefore, the high ductility is achieved. The weak texture and fine grains are mainly attributed to the higher ductility in the 1P alloy.

The bimodal structure containing fine DRX grains and coarse non-DRX regions can commendably alleviate the inconsistency between ductility and strength, as the existence of fine DRX grains is beneficial to the ductility improvement related to the increasing fraction of HAGBs and

Table 2 Deformation conditions and tensile properties of Al−Mg alloys

Alloy	Process	UTS/MPa	YS/MPa	δ/%	Source
Al−9.2Mg−0.8Mn−0.2Zr−0.15Ti	CR (4P)	531±6	350±1	10.0±2.0	This study
	HSRR (4P)	550±3	368±4	13.5±1.1	
	HSRR (2P)	507±9	308±6	24.9±1.3	
	HSRR (1P)	462±11	288±13	27.2±1.1	
Al−7Mg	ECAP	~507	~446	~14	[24]
Al−5.4Mg−0.5Mn	ECAP (300 °C)	415	335	24	[39]
Al−6.5Mg−0.5Sc	Extrusion (420 °C)	430	260	15	[48]
Al−7Mg−0.8Mn	Rapid solidification	436	270	25	[49]

stress relaxation. The 4P sample contains a high dislocation density as the recovery is the only softening process during the rolling process. The dislocation density in the 4P sample will quickly reach saturation during the tensile test. The work hardening rate drops obviously with the increased strain, and the stress concentration occurs rapidly, resulting in the low ductility. In comparison with the 4P sample, the 2P sample has the higher fraction of DRX, which is mainly related to the discontinuous dynamic recrystallization, and thus a higher work hardening rate with the strain above 0.06 is achieved. This reveals that a uniform stress distribution is obtained during the tensile test and the higher ductility is achieved. The non-DRX regions with high dislocation density provide enough dislocation strengthening and the fine Al_6Mn precipitates are also responsible for the high strength. The bimodal microstructure has been reported in the Al−Mg alloy and can simultaneously obtain high strength and large elongation. The high strength is ascribed to the ultrafine grains and the high ductility is due to the coarse grains relaxing the stress concentration [26,38].

To gain the ultrafine or nanostructured grains in Al alloy at elevated temperature is very difficult due to the active dynamic recovery. The deformation at room or low temperature and high strain accumulated by the multi-passes severe plastic deformation (SPD) processes is inappropriate to the Al−Mg alloy with high Mg content, i.e. ≥7% [14,24]. The plastic deformation followed by annealing is hard to obtain DRX grains with the size less than 10 μm by static recrystallization [52]. The annealing treatment also results in energy consumption and cost improvement. Therefore, achieving the bimodal structure by multi-passes of HSRR can act as an available method to achieve good balance of high strength and large ductility.

4 Conclusions

(1) The higher rolling reduction can effectively enhance the DRX process of the Al−9.2Mg−0.8Mn−0.2Zr−0.15Ti alloy. An elongated grain structure is formed in the alloy subjected to 4 passes of HSRR. An obvious bimodal grain distribution occurs in the alloy subjected to 2 passes of HSRR, in which the fine DRX grains with the average size of 6.4 μm and the coarse non-DRX regions with the average size of 47.7 μm are formed. The full DRX grain structure with the average grain size of 2.8 μm develops in the alloy subjected to 1 pass of HSRR.

(2) The improvement of θ_{AV} from 5.5° to 39.6° and the enhancement of the HAGBs fraction from 7.2% to 95.6% occur with the rolling pass ranging from 4 to 1. The texture intensity decreases from 9.55 to 1.65 with the HSRR pass ranging from 4 to 1 and a nearly random orientation develops with the annihilation of β-type fiber texture in the 1P alloy.

(3) The 4P alloy exhibits the highest strength but the lowest ductility, while the 1P alloy shows the largest elongation at the expense of strength. The 2P sample with the bimodal structure gains both high strength and large ductility, with the UTS of (507±9) MPa and the elongation to failure of (24.9±1.3)%. The formation of DRX grains and the weaker texture intensity are beneficial to the high ductility, which are related to the increasing fraction of HAGBs and stress relaxation. The high strength is mainly ascribed to dislocation strengthening due to the high dislocation density in the non-DRX regions and precipitation strengthening associated with the fine Al_6Mn particles.

Acknowledgments

The authors would like to express their sincere gratitude to Mr. YAN and Mr. WANG (Central South University, China) for their assistance in the TEM analysis and the uniaxial tensile testing.

References

[1] HUANG K, LOGÉ R E. A review of dynamic recrystallization phenomena in metallic materials [J]. Materials & Design, 2016, 111: 548−574.

[2] VETRANO J S, BRUEMMER S M, PAWLOWSKI L M, ROBERTSON I M. Influence of the particle size on recrystallization and grain growth in Al−Mg−X alloys [J]. Materials Science and Engineering A, 1997, 238: 101−107.

[3] NIKULIN I, KIPELOVA A, MALOPHEYEV S, KAIBYSHEV R. Effect of second phase particles on grain refinement during equal-channel angular pressing of an Al−Mg−Mn alloy [J]. Acta Materialia, 2012, 60: 487−497.

[4] FAN Cai-he, CHEN Xi-hong, ZHOU Xin-peng, OU Ling, YANG Jian-jun, PENG Ying-biao. Microstructure evolution and strengthening mechanisms of spray-formed 5A12 Al alloy processed by high reduction rolling [J]. Transactions of Nonferrous Metals Society of China, 2017, 27: 2363−2370.

[5] RADOVIC L, NIKACEVIC M, JORDOVIC B. Deformation behaviour and microstructure evolution of $AlMg_6Mn$ alloy during shear spinning [J]. Transactions of Nonferrous Metals Society of China, 2012, 22: 991−1000.

[6] SHE Xin-wei, JIANG Xian-quan, WANG Pu-quan, TANG Bin-bin, CHEN Kang, LIU Yu-jie, CAO Wei-nan. Relationship between microstructure and mechanical properties of 5083 aluminum alloy thick plate [J]. Transactions of Nonferrous Metals Society of China, 2020, 30: 1780−1789.

[7] YANUSHKEVICH Z, BELYAKOV A, KAIBYSHEV R. Microstructural evolution of a 304-type austenitic stainless steel during rolling at temperatures of 773−1273 K [J]. Acta Materialia, 2015, 82: 244−254.

[8] KAIBYSHEV R, SHIPILOVA K, MUSIN F, MOTOHASHI Y. Continuous dynamic recrystallization in an Al−Li−Mg−Sc alloy during equal-channel angular extrusion [J]. Materials Science and Engineering A, 2005, 396: 341−351.

[9] CAO Fu-rong, YIN Bin, LIU Si-yuan, SHI Lu, WANG Shun-cheng, WEN Jing-lin. Microstructural evolution, flow stress and constitutive modeling of Al−1.88Mg−0.18Sc−0.084Er alloy during hot compression [J]. Transactions of Nonferrous Metals Society of China, 2021, 31: 53−73.

[10] BLUM W, ZHU Q, MERKEL R, MCQUEEN H J. Geometric dynamic recrystallization in hot torsion of Al−5Mg−0.6Mn (AA5083) [J]. Materials Science and Engineering A, 1996, 205: 23−30.

[11] GALIYEV A, KAIBYSHEV R, GOTTSTEIN G. Correlation of plastic deformation and dynamic recrystallization in magnesium alloy ZK60 [J]. Acta Materialia, 2001, 49: 1199−1207.

[12] DEHGHAN M A, HODGSON P D. Dependency of recrystallization mechanism to the initial grain size [J]. Metallurgical and Materials Transactions A, 2008, 39: 2830−2840.

[13] LI Xin-yu, XIA Wei-jun, YAN Hong-ge, CHEN Ji-hua, SU Bin, SONG Min, LI Zhen-zhen, LI Ying-li. Dynamic recrystallization behaviors of high Mg alloyed Al−Mg alloy during high strain rate rolling deformation [J]. Materials Science and Engineering A, 2019, 753: 59−69.

[14] JIN Shen-bao, TAO Nai-rong, MARTHINSEN K, LI Yan-jun. Deformation of an Al−7Mg alloy with extensive structural micro-segregations during dynamic plastic deformation [J]. Materials Science and Engineering A, 2015, 628: 160−167.

[15] XU Guo-fu, CAO Xiao-wu, ZHANG Tao, DUAN Yu-lu. PENG Xiao-yan, DENG Ying, YIN Zhi-min. Achieving high strain rate superplasticity of an Al−Mg−Sc−Zr alloy by a new asymmetrical rolling technology [J]. Materials Science and Engineering A, 2016, 672: 98−107.

[16] SITDIKOV O, SAKAI T, AVTOKRATOVA E, KAIBYSHEV R, KIMURA Y, TSUZAKI K. Grain refinement in a commercial Al−Mg−Sc alloy under hot ECAP conditions[J]. Materials Science and Engineering A, 2007, 444: 18−30.

[17] LIU Jian-tao, DICK R E, FRIDY J M, ROUNS T N. Crystallographic texture evolution of continuous cast Al−Mn−Mg alloy sheet during cold rolling and annealing [J]. Materials Science and Engineering A, 2007, 458: 73−87.

[18] CHEN Ming-biao, LI Jing, ZHAO Ying-mei, YUAN Hui, LIU Wen-chang. Comparison of texture evolution between different thickness layers in cold rolled Al−Mg alloy [J]. Materials Characterization, 2011, 62: 1188−1195.

[19] GATTI J R, BHATTACHARJEE P P. Annealing textures of severely cold and warm-rolled Al−2.5wt.%Mg alloy [J]. Journal of Alloys and Compounds, 2014, 615: 950−960.

[20] LIU Wen-chang, LI Jing, YUAN Hui, YANG Qing-xiang. Effect of recovery on the recrystallization texture of an Al−Mg alloy [J]. Scripta Materialia, 2007, 57: 833−836.

[21] ENGLER O. An EBSD local texture study on the nucleation of recrystallization at shear bands in the alloy Al−3%Mg [J]. Scripta Materialia, 2001, 44: 229−236.

[22] LIN Jin-bao, WANG Xin-yi, REN Wei-jie, YANG Xue-xia, WANG Qu-dong. Enhanced strength and ductility due to microstructure refinement and texture weakening of the GW102K alloy by cyclic extrusion compression [J]. Journal of Materials Science and Technology, 2016, 32: 783−789.

[23] SITDIKOV O, SAKAI T, AVTOKRATOVA E, KAIBYSHEV R, TSUZAKI K. Microstructure behavior of Al−Mg−Sc alloy processed by ECAP at elevated temperature [J]. Acta Materialia, 2008, 56: 821−834.

[24] ZHA Min, LI Yan-jun, MATHIESEN R H, BJØRGE R, ROVEN H J. Microstructure evolution and mechanical behavior of a binary Al−7Mg alloy processed by equal-channel angular pressing [J]. Acta Materialia, 2015, 84: 42−54.

[25] HUO Wang-tu, SHI Jin-tao, HOU Long-gang, ZHANG Ji-shan. An improved thermo-mechanical treatment of high-strength Al−Zn−Mg−Cu alloy for effective grain refinement and ductility modification [J]. Journal of Materials Processing Technology, 2017, 239: 303−314.

[26] JIN H, LLOYD D J. Effect of a duplex grain size on the tensile ductility of an ultrafine grained Al−Mg alloy, AA5754,

produced by asymmetric rolling and annealing [J]. Scripta Materialia, 2004, 50: 1319−1323.

[27] LIU M P, ROVEN H J, MURASHKIN M Y, VALIEV R Z, KILMAMETOV A, ZHANG Z, YU Y D. Structure and mechanical properties of nanostructured Al−Mg alloys processed by severe plastic deformation [J]. Journal of Materials Science, 2013, 48: 4681−4688.

[28] ZHA Min, LI Yan-jun, MATHIESEN R H, BJØRGE R, ROVEN H J. High ductility bulk nanostructured Al−Mg binary alloy processed by equal channel angular pressing and interpass annealing [J]. Scripta Materialia, 2015, 105: 22−25.

[29] LIN Jun-ping. Effect of Mg content on dynamic recrystallization behaviours of Al−Mg alloys [J]. Journal of University of Science and Technology Beijing, 1997, 19: 47−51.

[30] LEE Y B, SHIN D H, PARK K T, NAM W J. Effect of annealing temperature on microstructures and mechanical properties of a 5083 Al alloy deformed at cryogenic temperature [J]. Scripta Materialia, 2004, 51: 355−359.

[31] LIU Xiang-yang, ADAMS J B. Grain-boundary segregation in Al−10%Mg alloys at hot working temperature [J]. Acta Metallurgica, 1998, 46: 3467−3476.

[32] BENSON R B, WITHROW S P, PENNYCOOK S J. Formation of an Al_6Mn precipitate in aluminum annealed after implantation with 3.5 atomic percent manganese [J]. Materials Letters, 1988, 6: 93−95.

[33] NAKAYASU H, KOBAYASHI E, SATO T, HOLMESTAD R, MARTHINSEN K. Orientation relationships of phase transformation in alpha-$Al_{12}Mn_3Si$ pseudomorphs after plate-like Al_6Mn precipitate in an AA3004 Al−Mn based alloy [J]. Materials Characterization, 2018, 136: 367−374.

[34] KIMURA K, HASHIMOTO T, SUZUKI K, NAGAYAMA K, INO H, TAKEUCHI S. Structure and stability of quasicrystalline Al−Mn alloys [J]. Journal of the Physical Society of Japan, 2007, 55: 534−543.

[35] NAM N D, PHUNG V D, THUY P T P, DAO V A, KIN S H, YI J S. Corrosion behaviours of hot-extruded Al−xMg alloys [J]. Journal of Materials Research and Technology, 2019, 8: 5246−5253.

[36] CHOI D H, AHN B W, QUESNEL D J, JUNG S B. Behavior of β phase (Al_3Mg_2) in AA 5083 during friction stir welding [J]. Intermetallics, 2013, 35: 120−127.

[37] WU Yuan-zhi, YAN Hong-ge, CHEN Ji-hua, DU Yong-guo, ZHU Su-qin. Microstructure and mechanical properties of ZK21 magnesium alloy fabricated by multiple forging at different strain rates [J]. Materials Science and Engineering A, 2012, 556: 164−169.

[38] WITKIN D, LEE Z, RODRIGUEZ R, NUTT S, LAVERNIA E. Al−Mg alloy engineered with bimodal grain size for high strength and increased ductility [J]. Scripta Materialia, 2003, 49: 297−302.

[39] MALOPHEYEV S, KAIBYSHEV R. Strengthening mechanisms in a Zr-modified 5083 alloy deformed to high strains [J]. Materials Science and Engineering A, 2015, 620: 246−252.

[40] KAIBYSHEV R, AVTOKRATOVA E, SITDIKOV O. Effect of intense plastic straining on microstructure and mechanical properties of an Al−Mg−Sc alloy [J]. Journal of Physics: Conference Series, 2010, 240: 012120.

[41] LI Xin-yu, XIA Wei-jun, YAN Hong-ge, CHEN Ji-hua, SU Bin, SONG Min, LI Zhen-zhen, LU Yang. High strength and large ductility of a fine-grained Al−Mg alloy processed by high strain rate hot rolling and cold rolling [J]. Materials Science and Engineering A, 2020, 787: 139481.

[42] XIAO Han, LU Zhen, ZHANG Kai-feng, JIANG Shao-song, SHI Cheng-cheng. Achieving outstanding combination of strength and ductility of the Al−Mg−Li alloy by cold rolling combined with electropulsing assisted treatment [J]. Materials & Design, 2020, 186: 108279.

[43] SURESH M, SHARMA A, MORE A M, KALSAR R, BISHT A, NAYAN N, SUWAS S. Effect of equal channel angular pressing (ECAP) on the evolution of texture, microstructure and mechanical properties in the Al−Cu−Li alloy AA2195 [J]. Journal of Alloys and Compounds, 2019, 785: 972−983.

[44] ZHOU Fei, LIAO Xiao-zhou, ZHU Yun-tian, DALLEK S, LAVERNIA E J. Microstructural evolution during recovery and recrystallization of a nanocrystalline Al−Mg alloy prepared by cryogenic ball milling [J]. Acta Materialia, 2003, 51: 2777−2791.

[45] LEE Y B, SHIN D H, PARK K T, NAM W J. Effect of annealing temperature on microstructures and mechanical properties of a 5083 Al alloy deformed at cryogenic temperature [J]. Scripta Materialia, 2004, 51: 355−359.

[46] DENG Ying, ZHANG Guo, YANG Zi-ang, XU Guo-fu. Microstructure characteristics and mechanical properties of new aerospace Al−Mg−Mn alloys with $Al_3(Sc_{1-x}Zr_x)$ or $Al_3(Er_{1-x}Zr_x)$ nanoparticles [J]. Materials Characterization, 2019, 153: 79−91.

[47] LIU K, CHEN X G. Evolution of microstructure and elevated-temperature properties with Mn addition in Al−Mn−Mg alloys [J]. Journal of Materials Research, 2017, 32: 2585−2593.

[48] DRITS M E, TOROPOVA L S, BYKOV Y G. Effect of REM on the mechanical properties of aluminum alloys containing 6.5% Mg [J]. Metal Science and Heat Treatment, 1980, 22: 743−745.

[49] MAENG D Y, LEE J H, HONG S I, CHUN B S. Microstructure and mechanical properties of rapidly solidified Al−7wt.%Mg−X (X=Cr, Zr or Mn) alloys [J]. Materials Science and Engineering A, 2001, 311: 128−134.

[50] DUCKHAM A, KNUTSEN R D, ENGLER O. Influence of deformation variables on the formation of copper-type shear bands in Al−1Mg [J]. Acta Materialia, 2001, 49: 739−749.

[51] ZHU Su-qin, YAN Hong-ge, CHEN Ji-hua, WU Yuan-zhi, LIU Ji-zi, TIAN Jin. Effect of twinning and dynamic recrystallization on the high strain rate rolling process [J]. Scripta Materialia, 2010, 63: 985−988.

[52] MA Peng-cheng, ZHANG Di, ZHUANG Lin-zhong, ZHANG Ji-shan. Effect of alloying elements and processing parameters on the Portevin−Le Chatelier effect of Al−Mg alloys [J]. International Journal of Minerals, Metallurgy Materials, 2015, 22: 175−183.

高 Mg 含量 Al−Mg 合金高应变速率轧制变形下的动态再结晶、织构和力学性能

黎新宇[1,2]，夏伟军[1,2]，陈吉华[1,2]，严红革[1,2]，李贞贞[1,2]，苏 斌[1,2]，宋 旼[3]

1. 湖南大学 材料科学与工程学院，长沙 410082；
2. 湖南大学 湖南省喷射沉积技术与应用重点实验室，长沙 410082；
3. 中南大学 粉末冶金国家重点实验室，长沙 410083

摘 要：对高 Mg 含量 Al−Mg 合金(Al−9.2Mg−0.8Mn−0.2Zr−0.15Ti，质量分数，%)进行不同道次(1，2 和 4)高应变速率轧制变形，终轧变形量、轧制温度和应变速率分别为 72%、400 °C 和 8.6 s^{-1}。采用光学显微镜、扫描电镜、电子背散射衍射技术和透射电镜研究合金的组织演变。合金经 2 道次高应变速率轧制变形后获得明显的双峰组织，其中细小再结晶晶粒和未再结晶组织的平均尺寸分别为 6.4 和 47.7 μm。合金具有高的抗拉强度((507±9) MPa)和伸长率((24.9±1.3)%)。在 2 道次高应变速率轧制变形过程中，晶界非连续动态再结晶为合金主要的再结晶机制。

关键词：Al−Mg 合金；高应变速率轧制；双峰组织；动态再结晶

(Edited by Wei-ping CHEN)